3D printability of recycled steel fibre-reinforced ultra-high performance concrete

Meng Chen [a,b], Jiahui Li [a], Tong Zhang [a,*], Mingzhong Zhang [c]

[a] *School of Resources and Civil Engineering, Northeastern University, Shenyang 110819, China*
[b] *Institute for Frontier Technologies of Low-Carbon Steelmaking, Northeastern University, Shenyang 110819, China*
[c] *Department of Civil, Environmental and Geomatic Engineering, University College London, London WC1E 6BT, UK*

Keywords:
3D concrete printing
Ultra-high performance concrete
Recycled steel fibre
Rheology
Extrudability
Buildability

A B S T R A C T

3D printing ultra-high performance concrete (UHPC) can be used for additive construction of structural components, which significantly reduces the reliance on steel reinforcement. This study investigates the effects of water-to-binder (w/b) ratios, recycled steel fibre (RSF) volume fraction and thickener content on the rheological behaviour, flowability, extrudability, buildability and shape retention ability of 3D printing RSF-reinforced UHPC. The results show that decreasing the w/b ratio, RSF incorporation and thickener incorporation increase the static and dynamic yield stress of the mixture. The dynamic yield stress of the mixture increases by 27.37 % when the volume fraction of RSF is increased from 1 % to 3 % at the same w/b ratio and thickener content. The addition of thickener increases the extrudability and buildability of 3D printing RSF-reinforced UHPC, which is mainly related to the adsorption of the thickener on the surface of the cementitious material particles and the introduction of bridging forces in the system of neighbouring cementitious material particles. The shape retention ability of 3D printing RSF-reinforced UHPC can be improved by increasing RSF volume fraction and thickener content. In addition, the mixture with a w/b ratio of 0.16, RSF volume fraction of 3 % and thickener content of 0.1 % shows the best printability.

1. Introduction

3D concrete printing is an innovative construction method that utilises cement-based materials and high-precision layer-by-layer stacking techniques to build complex and robust structures. This technology not only greatly improves the efficiency of construction, but also significantly reduces the loss of building materials, which is a crucial technological innovation to promote the greening of the construction industry and reduce its carbon footprint [1–3]. First, it offers a high degree of design freedom, enabling complex geometries and structures to be realized to meet individualized and customized requirements [4, 5]. Second, it reduces material waste and improves material utilization by precisely controlling the use of materials [6–8]. The automated printing process significantly shortens the construction cycle and improves construction efficiency, while reducing labour costs and construction risks [9]. In addition, 3D concrete printing allows the use of environmentally friendly materials, reducing the impact on the environment and meeting sustainable development requirements. However, it has not been able to completely replace traditional reinforced concrete structures due to its inability to provide tensile strength with built-in steel reinforcement, limiting its wide application in large-scale construction projects [10–12].

Ultra-high performance concrete (UHPC) is an advanced concrete material with an extremely compact microstructure that significantly reduces the risk of porosity and infiltration, resulting in extremely high compressive strength and durability [13–16]. The integration of fibre-reinforced concrete and 3D concrete printing technology can compensate for the current problem of insufficient reinforcement in 3D concrete printing [17,18]. Currently, many attempts are being made to develop 3D printing technology for UHPC, and increasing attention is being paid to the printability and static mechanical properties of 3D printing UHPC [19,20]. For instance, the printing of UHPC specimens has excellent flexural properties due to the preferential alignment of steel fibre oriented along the printing direction [21]. Under the same impact velocity conditions, the elastic modulus and strain rate effect of the 3D printing UHPC specimens exhibit anisotropic characterization, which is attributed to their varying elastic moduli in different directions [22]. In addition, it has been verified the feasibility of 3D printing UHPC

* Corresponding author. *E-mail address:* zhangtong@mail.neu.edu.cn (T. Zhang)

as a reinforcing material for concrete members [23,24].

However, it is undeniable that in practical large-scale applications, 3D printing UHPC is similar to conventional UHPC with high costs, leading to their inability to be used on a large scale. As an integral part of UHPC, steel fibre plays a crucial role in enhancing the overall performance of the material. However, the high cost of industrial steel fibre (ISF) hinders the large-scale popularization and application of UHPC [25]. Recycled steel fibre (RSF) can exhibit similar physical and mechanical behaviours as ISF, while the costs of RSF are approximately one-tenth of those of ISF, highlighting the obvious cost advantage of RSF [26,27]. Therefore, the use of RSF to partially or completely replace ISF in UHPC and the study of its impact on the mechanical properties of UHPC has received wide attention. For example, the tensile strength of RSF-reinforced concrete is found to be even better than that of ISF-reinforced concrete [28], and RSF can significantly improve the flexural capacity of concrete [29,30]. It has been shown that the engineering properties of concrete reinforced with RSF are comparable to those of concrete reinforced with ISF [31,32]. Moreover, the dynamic splitting strength and energy dissipation capacity of UHPC increase when the RSF content is lower than 3.0 % [27]. Although current studies have focused on the mechanism of RSF action in conventional UHPC, the influence of RSF on the printability of 3D printing UHPC is still unclear. Therefore, elucidating the printable properties of 3D printing RSF-reinforced UHPC and its mechanism of action is the basis for its further application.

This study aims to comprehensively examine the printability of 3D printing RSF-reinforced UHPC. Different water-to-binder (w/b) ratios, RSF volume fraction and content of thickener were used to prepare 3D printing RSF-reinforced UHPC. The printability of 3D printing RSF-reinforced UHPC was investigated by rheological behaviour, extrudability, buildability and shape retention ability tests on the mixture. Finally, the mechanism of RSF and thickener on the printability of 3D printing RSF-reinforced UHPC was analysed. This study could promote the research progress of printing RSF-reinforced UHPC and provide a reference for the development of environmentally friendly 3D printing UHPC.

2. Experimental programs

2.1. Raw materials

P.O. 52.5 ordinary Portland cement and silica fume were utilised as binders. For fine aggregate, quartz sand with a density of 2.65 g/cm^3 and particle size of 0.1–0.6 mm was used. The particle size distribution of binders and fine aggregate in 3D printing RSF-reinforced UHPC is shown in Fig. 1. The admixtures included both polycarboxylate-based superplasticizers (SP) and hydroxypropyl methylcellulose-based viscosity-modified admixture (VMA) thickeners.

This study used RSF as fibre. RSF was provided by a Chinese tyre recycling company. Since the geometry of RSF was irregularly wavy, the distance between the two ends of RSF was defined as the fibre length [33–35]. Fig. 2 shows the distribution of RSF lengths based on 1000 RSF. After statistical analysis, the minimum length of RSF was 3.3 mm, the maximum length was 17.8 mm, and the average length was about 12.59 mm. Table 1 lists the physical and mechanical properties of RSF.

2.2. Mix proportions

Table 2 shows the mix proportions of 3D printing RSF-reinforced UHPC. The mix ratios were based on those used in the previous studies [24,27,36] and were adjusted by pre-testing. The mass ratio of cement and silica fume in the binders was close to 8:2, and the quartz sand-to-binder mass ratio was close to 1.11:1. In order to investigate the effects of w/b ratio, RSF volume fraction, and VMA content on the printability of 3D printing RSF-reinforced UHPC. The w/b ratios were set to 0.14, 0.16 and 0.18, respectively. In pre-testing, it was found that a

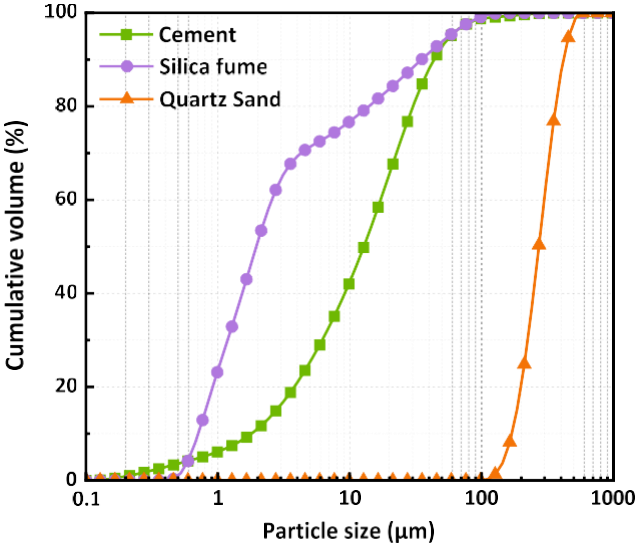

Fig. 1. Particle size analysis of the binders and fine aggregate in 3D printing mixture.

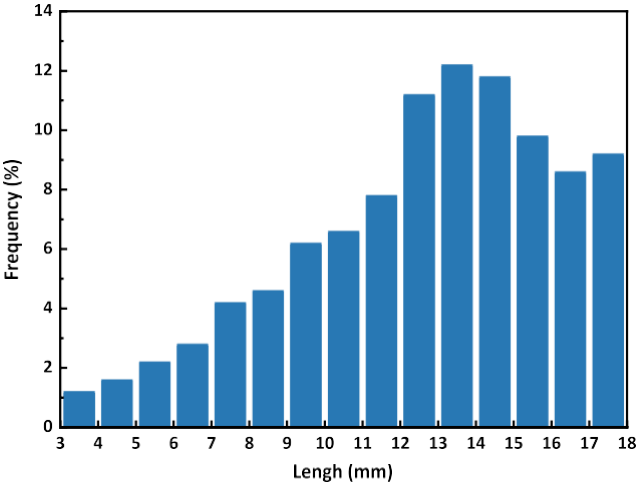

Fig. 2. Length distribution of RSF.

Table 1
Characterization and mechanical properties of RSF.

Fibre appearance	Length (mm)	Diameter (mm)	Tensile strength (MPa)	Elastic modulus (GPa)
	3.3–17.8	0.22	2165	200

Table 2
Mix proportions of 3D printing RSF-reinforced UHPC (kg/m³).

Mixture ID	Cement	Silica fume	Quartz sand	Water	SP	VMA	RSF
W14R3V0.1	788	200	1100	138	10	1	234
W16R3V0.1	788	200	1100	158	10	1	234
W18R3V0.1	788	200	1100	177	10	1	234
W16R1V0.1	788	200	1100	158	10	1	78
W16R2V0.1	788	200	1100	158	10	1	156
W16R3V0.05	788	200	1100	158	10	0.5	234
W16R3V0.2	788	200	1100	158	10	2	234

mixture of 4 % RSF by volume clogged the print head during printing. Therefore, RSF was incorporated into the mixture at 1 %, 2 % and 3 % volume fractions, respectively. The mass ratios of VMA to binders were 0.05 %, 0.10 % and 0.20 %, respectively.

2.3. Sample preparation

A six-axis robotic arm 3D printer was used for the experiment. The size of the printer is 3000 mm (L) × 1100 mm (W) × 1500 mm (H), the print nozzle was a circular nozzle that was 20 mm in diameter, and the maximum arm span of the robot arm was 1722 mm, as shown in Fig. 3. The printing speed of the printer as well as the extrusion speed in the experiment were referred to the previous study [37] and followed the results of pre-tests. Accordingly, the moving and extrusion speeds of the 3D concrete printer were set as 60 mm/s and 1.5 L/min, respectively.

Sample preparation was divided into six steps: (1) Cement, silica fume, and quartz sand were poured into a mixer in proportion to the mixture for about 3 min to make the mixture homogeneous in the pot. (2) RSF was then added slowly into a pot and stirred for 2 min to make RSF evenly distributed in the mixture. (3) Half of the water and all of the SP were slowly poured into the pot and stirred for about 3 min. (4) All remaining water was poured into the pot and stirred for about 2 min. (5) The VMA was added for 2 min. (6) Finally, the mixture was mixed at high speed for 3 min.

2.4. Test methods

2.4.1. Rheological test

In order to assess the impact of w/b ratio, RSF volume fraction and VMA content on the rheological behaviour of 3D printing RSF-reinforced UHPC, the rheological behaviour of the mixture was measured using a NELD-CRV610 rheometer. The blade radius and height were 34.5 mm and 69 mm respectively and the blade probe consisted of four blades. The outer cylinder was a 3.6 L volume rheometer vessel. After the materials were prepared and mixed, the fresh mixture was poured into a container. To measure the static yield stress using the stress-growth test, a steady rate of 0.025 rps was applied to the mixture for 60 s. The change in torque during rotation was observed and the maximum torque value was taken to calculate the static yield stress of the mixture [38]. After 10, 20, 30, 40, 50 and 60 min of resting, the static yield stress of the mixture was measured.

Dynamic yield stress was performed using a rheological curve test. The rheological scheme is shown in Fig. 4. The mixture was pre-sheared at 0.6 rps for 40 s and then the applied shear rate was gradually decreased [39]. Rheological curves were fitted using the Bingham model [40] for determining the dynamic yield stress and plastic viscosity in 3D printing RSF-reinforced UHPC. To minimize the effect of errors, all mixtures were visually inspected at the end of the rheological test to check and confirm that no sand or fibre was separated from the mixture [41,42].

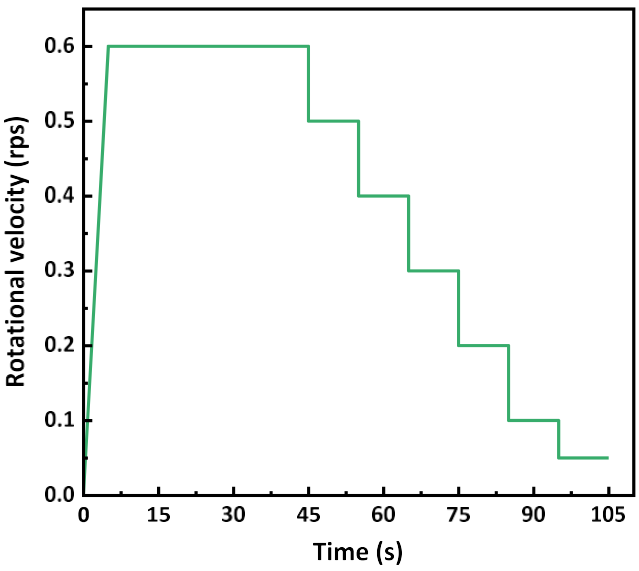

Fig. 4. Variation curve of rotational speed with time in the rheological curve test.

$$\tau = \tau_0 + \mu\dot{\gamma} \quad (1)$$

where τ is the shear stress; τ_0 and μ stand for the dynamic yield stress and plastic viscosity, respectively; and $\dot{\gamma}$ represents the shear rate.

2.4.2. Flowability test

The slump flow test was utilised to characterize the flow evolution of 3D printing RSF-reinforced UHPC, and the slump test was performed using a conical mould following the Chinese standard for cement mortar flow determination [43]. The conical mould used in the test was 60 mm in height, 60 mm in diameter at the top and 100 mm at the bottom. The slump test was carried out by rapidly filling the mould with the mixture in two stages. Subsequently, the mould was removed and the slump value was recorded as an evaluation criterion for the extrudability and buildability test open time of the 3D printing mixture. Subsequently, the table was shaken 25 times, the diameter of the mixture was recorded and the average of the two orthogonal diameters was taken as the slump flow

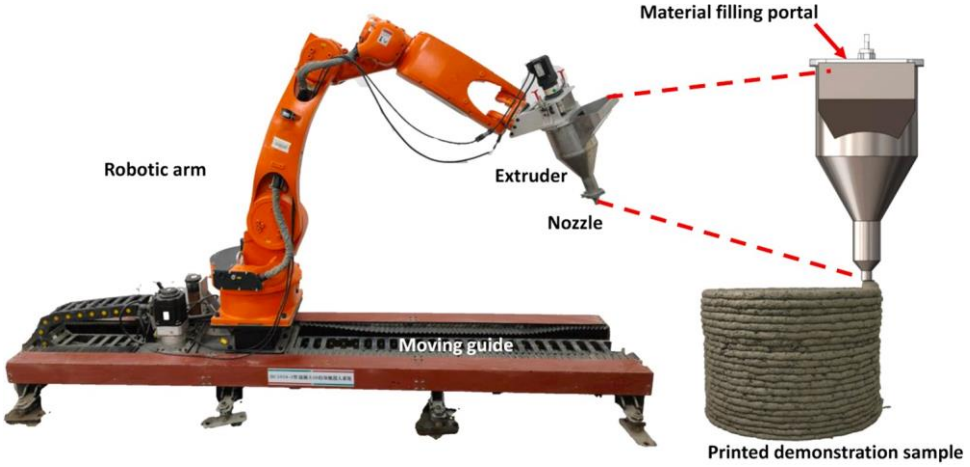

Fig. 3. Schematic diagram of 3D concrete printing equipment.

value. The test was carried out at 10-minute intervals within 60 min of sampling.

2.4.3. Extrudability test

The extrudability of the 3D printing RSF-reinforced UHPC was the ability to extrude continuously and smoothly through a nozzle. Therefore, the extrudability test included two aspects:

(1) Printable time test: The print time test was a print of a 500 mm length of single filament at various resting times. This process was continued (test every 10 min up to 60 min, every 15 min between 60 and 120 min, every 30 min between 120 and 180 min, and a final test after 240 min of resting if the wire has not broken) until filament breakage was observed. The time of maximum rest until filament breakage was recorded as printable time [44].
(2) Printable filament conformability test: Stable extrusion filament geometry was very important for the quality of 3D printing structures, especially in the case of lengthy contours. The conformability of the printing filament was assessed by comparison of the design width and actual width. In this test, the extrudability shape retention ability of the filament was assessed by printing 20 mm wide filaments in five groups of one to five filaments each. The length of each filament was 300 mm, and the total continuous extruded filament length in the test was 4500 mm [45].

2.4.4. Buildability test

Because there was no formwork throughout the 3D printing process, the extruded filament needed to be able to withstand the force of gravity as well as the weight of the subsequently deposited filament. In this case, the capacity of the extruded filament to maintain its shape reflects the buildability of the mixture. Buildability was evaluated by two methods:

(1) Buildable layer test: The buildability was evaluated by printing a hollow cylinder with a diameter of 300 mm using different mixtures. The layer height of the hollow cylinder was 10 mm. The maximum layers and height of the deposit before collapse were recorded as an indicator to assess the buildability of the mixture [46].
(2) The layer settlement test: The test was to print a test object with five pairs of stacked layers. The five-layer test object was designed to have a length of 700 mm, a width of 20 mm and a height of 50 mm. The buildability was evaluated by calculating the shape stability ratio (S) of the actual print height (H) to the design height (h) of the test object [47].

2.4.5. Shape retention ability test

Shape retention ability (SRA) is the ability of a fresh mixture to retain its shape after extrusion [21]. The mixture was loaded in two batches in a plastic cylinder 60 mm in diameter and height, tamped gently, and then lifted the cylinder. A plastic plate having a side length of 100 mm and weighing 10 g was gently placed on the top of the mixture, and then two round steel plates were placed in turn on top of the mixture to distribute the pressure evenly over the mixture until the plastic sheet came off. The circular steel plate was 60 mm in diameter and weighed 170 g. The mixture was recorded with a camera with images of each loading stage. Height and diameter measurements of the mixture at the end of the test were also taken to quantitatively assess the SRA of the mixture. The SRA of fresh 3D printing RSF-reinforced UHPC was defined in Eq. (2). SRA_d and SRA_h reflected the size changes in the diameter and height of the 3D printing RSF-reinforced UHPC sample, respectively.

$$SRA_d = \frac{d_L}{d} \text{ and } SRA_h = \frac{h_L}{h} \quad (2)$$

where h_L and d_L are the bottom height and diameter of a 3D printing RSF-reinforced UHPC sample for a specified load L and h, d are the bottom height and diameter of the 3D printing mixture specimen before loading.

3. Results and discussions

3.1. Rheological behaviour

3.1.1. Static yield stress

The static yield stress is essential to the rheological behaviour of printing concrete [48,49]. Fig. 5 shows the results of static yield stress over time for 3D printing RSF-reinforced UHPC. For all 3D printing mixtures, the static yield stress increases with increasing resting time. In 30 min the static yield stress increases relatively slowly and then increases more rapidly after 30 min. This is essentially because as the hydration time increases, the generation of hydration products such as C-S-H gels act as connecting bridges among the particles enhancing the flocculation structure [50], which leads to a gradual increase in the static yield stress.

Fig. 5(a) shows the influence of the w/b ratio on the static yield stress of the 3D printing mixture, which reduces with increasing w/b ratio. When the w/b ratio is increased from 0.14 to 0.18, the static yield stress of the mixture decreases by 52.65 % at a rest time of 30 min. This is mainly because increasing the w/b ratio greatly reduces viscous resistance during flow deformation of the 3D printing mixture, which leads to a reduction in static yield stress [51]. The effect of RSF content on static yield stress is shown in Fig. 5(b). When the RSF volume fraction is increased from 1 % to 3 %, the static yield stress of the mixture at 40 min of rest is increased from 530.677 Pa to 2044.674 Pa. The incorporation of RSF increases the static yield stress of the mixture, which can be explained by the reason that the stiffness of RSF enhances that of the 3D printing mixture [46]. Fig. 5(c) shows the effect of VMA content on the static yield stress of the mixture. The static yield stress of the mixture increases with increasing VMA content. With increasing VMA content from 0.05 % to 0.2 %, the static yield stress of the mixture at a rest time of 60 minutes increases by 60.99 %. VMA increases the static yield stress of the mixture mainly by adsorbing to the surface and introducing bridging forces in the system of neighbouring cementitious material particles [52].

3.1.2. Dynamic yield stress and plastic viscosity

Fig. 6 shows the experimental results of the rheological curve of the mixture, and the dynamic yield stress and plastic viscosity of 3D printing RSF-reinforced UHPC are obtained by fitting these curves to the Bingham model, as shown in Table 3. The dynamic yield stress of concrete indicates the minimum stress exerted when the concrete is in the flow state [53], while the plastic viscosity reflects the size of the internal friction of the concrete when the flow occurs [50]. Similar to the results for static yield stress, the dynamic yield stress of the mixture also decreases gradually with the increase of the w/b ratio. This is mainly due to the fact that the increasing w/b ratio greatly improves the flowability of the 3D printing mixture and reduces the viscous resistance to flow deformation. This leads to a decrease in plastic viscosity and dynamic yield stress of the mixture [51]. As the w/b ratio increases, the dynamic yield stress and plastic viscosity of the mixture decrease, and the extrudability of the mixture becomes better. With increasing RSF volume fraction, the dynamic yield stress of the mixture increases gradually. The dynamic yield stress of the mixture with a 3 % volume fraction of RSF increases by 27.37 % relative to the mixture with a 1 % volume fraction of RSF. This is because the friction between RSF and the interaction of RSF with solid material decreases the packing density of the UHPC matrix. On the other hand, as the RSF volume fraction increases, it leads to an increase in the possibility of RSF interlocking [42,54]. In addition, the plastic viscosity of 3D printing RSF-reinforced UHPC increases with the increase of VMA content. The plastic viscosity of the mixture increases by 29.04 % as the VMA content increases from 0.05 %

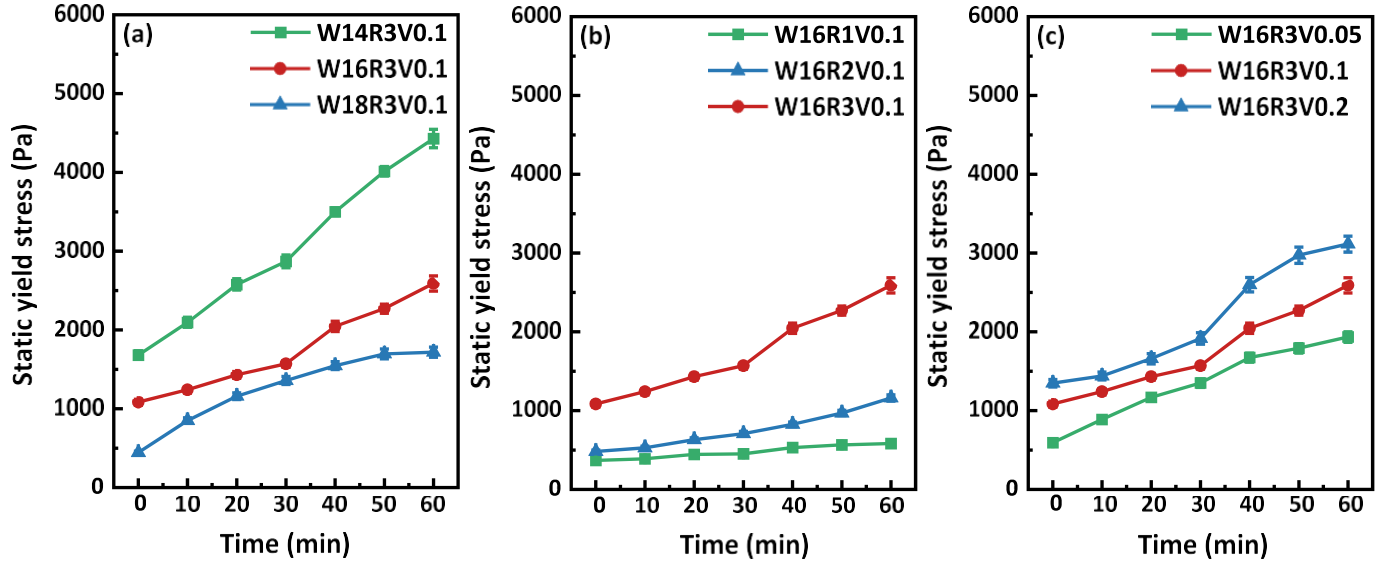

Fig. 5. Variation of static yield stress with time of 3D printing mixture.

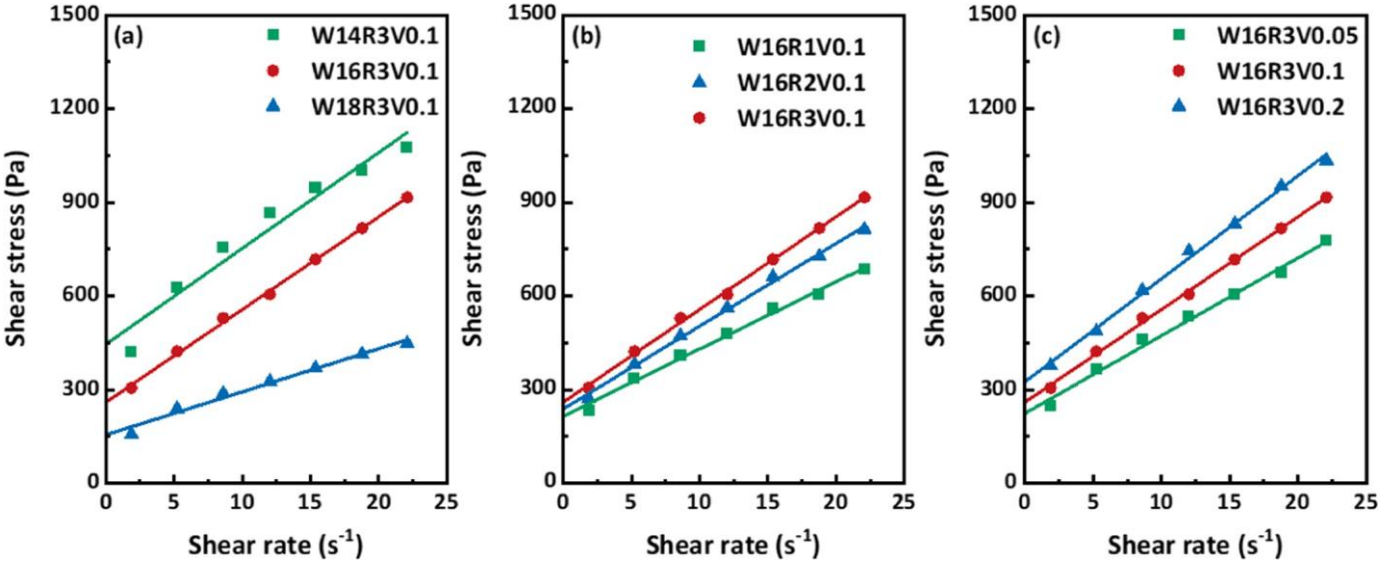

Fig. 6. Rheological curve fits for 3D printing RSF-reinforced UHPC.

Table 3
Dynamic yield stress and plastic viscosity of 3D printing mixture.

Group	Dynamic yield stress (Pa)	Plastic viscosity (Pa·s)	R^2
W14R3V0.1	549.705	192.813	0.954
W16R3V0.1	351.416	170.540	0.997
W18R3V0.1	194.455	85.006	0.976
W16R1V0.1	275.893	128.024	0.991
W16R2V0.1	341.406	149.865	0.992
W16R3V0.05	288.437	147.474	0.989
W16R3V0.2	435.808	190.303	0.997

to 0.2 %. This is mainly because the inclusion of VMA leads to an increase in plastic viscosity in cement paste [55]. Increasing the content of RSF and VMA increases the dynamic yield stress and the plastic viscosity of the mixture, which is detrimental to the extrusion of the mixture.

3.2. Flowability

Fig. 7 shows the influence of different influencing factors for 3D printing RSF-reinforced UHPC flowability. Fig. 7(a) shows the influence of the w/b ratio for 3D printing RSF-reinforced UHPC flowability. Overall, the flowability of all the 3D printing mixtures decreases with increasing rest time. The nucleation of early hydration products on the surface of un-hydrated particles induces the formation of a compact flocculent structure between the particles, which reduces the flowability of the slurry [56]. Whereas, with the increase in w/b ratio, there is a significant increase in the flowability of the mixture. At a rest time of 20 min, the spread diameter increases from 115 mm to 151 mm following an increase in w/b ratio from 0.14 to 0.18. This is mainly because the 3D printing RSF-reinforced UHPC is designed using a very low w/b ratio, and the addition of a small amount of water can have a large impact on the flowability performance with the same content of binders.

Fig. 7(b) shows the influence of RSF volume fraction for 3D printing

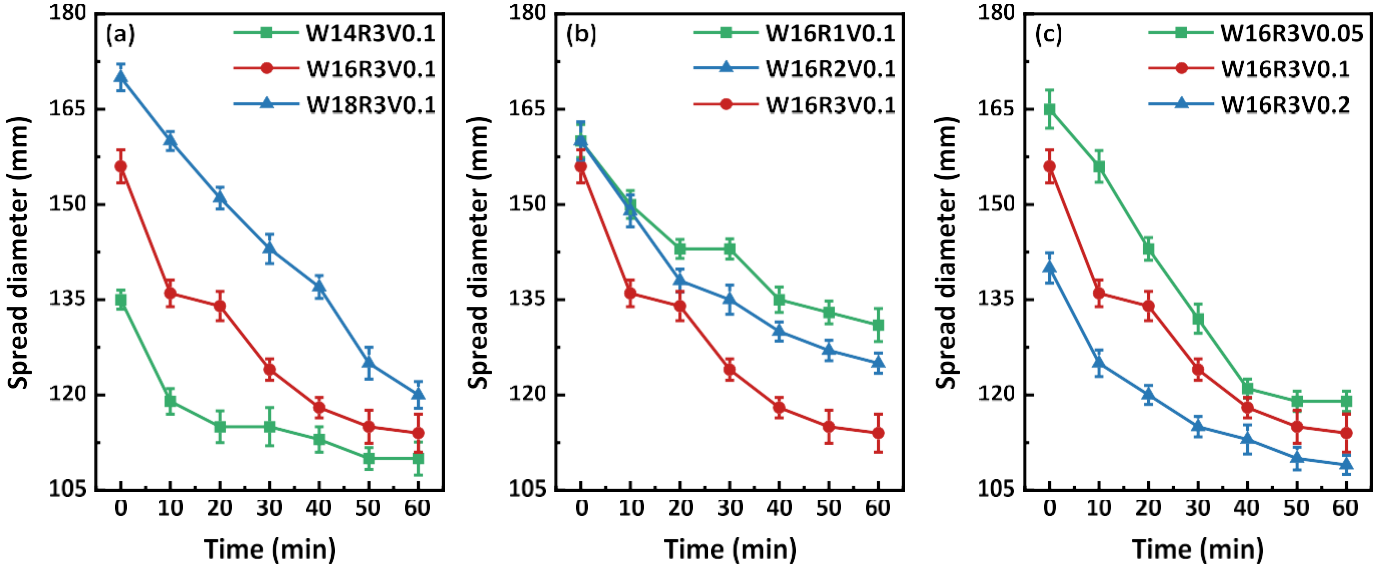

Fig. 7. Flow test results of mixtures with different influencing factors at different times.

RSF-reinforced UHPC flowability. The flowability of the mixture decreases with increasing fibre content and there is a significant difference in the spread diameter of the mixture after 30 min. The major reason for this is that as RSF content increases, the interaction between RSF increases, and the RSF cross-lap forms a complex three-dimensional disordered system inside the mixture, which supports the skeleton and hinders the diffusion of the mortar body. In addition, the friction between the RSF and RSF as well as the friction between the RSF and the slurry also affects the diffusion of the slurry [57]. Fig. 7(c) shows the influence of VMA content for 3D printing RSF-reinforced UHPC flowability. The flowability of the mixture decreases as the VMA content increases. At a rest time of 40 min, the spreading diameter of the mixture with a VMA content of 0.2 % decreases by 6.61 % compared to the mixture with a VMA content of 0.05 %. This may be due to the nature of VMA which increases the cement paste viscosity and also improves the internal friction of the paste which in turn increases the yield stress and plastic viscosity of the paste. Therefore, the addition of VMA to 3D printing RSF-reinforced UHPC decreases the flowability of concrete [58].

The test results of 3D printing RSF-reinforced UHPC slump are shown in Fig. 8. Decreasing the w/b ratio, increasing the RSF volume fraction, or increasing the VMA content can reduce the slump. With a lower slump, the buildability of 3D printing mixtures is higher [59]. Fresh mortars with a slump of less than 8 mm have satisfactory buildability [60]. The results show that the slump of all the mixtures is below 8 mm within 60 min, except for the mixtures of W16R3V0.05 and W18R3V0.1 with the slump falling below 8 mm at 20 min. Therefore, the results indicate that the opening time for reasonable extrudability and constructability testing of 3D printing RSF-reinforced UHPC should be after 20 min.

3.3. Extrudability

3.3.1. Printable time

Table 4 shows a schematic of the printable time for all 3D printing mixtures. The results show that the printable time of the mixture

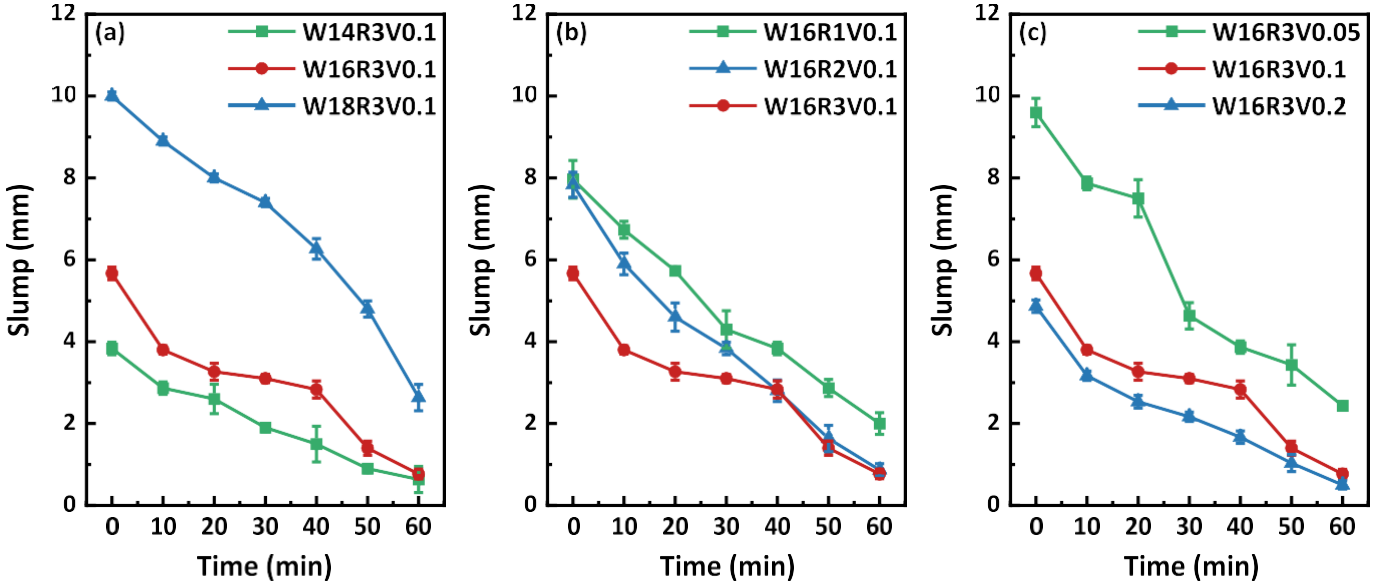

Fig. 8. Slump test results of mixtures with different influencing factors at different times.

Table 4
Schematic photos of all 3D printing mixtures at various printing times.

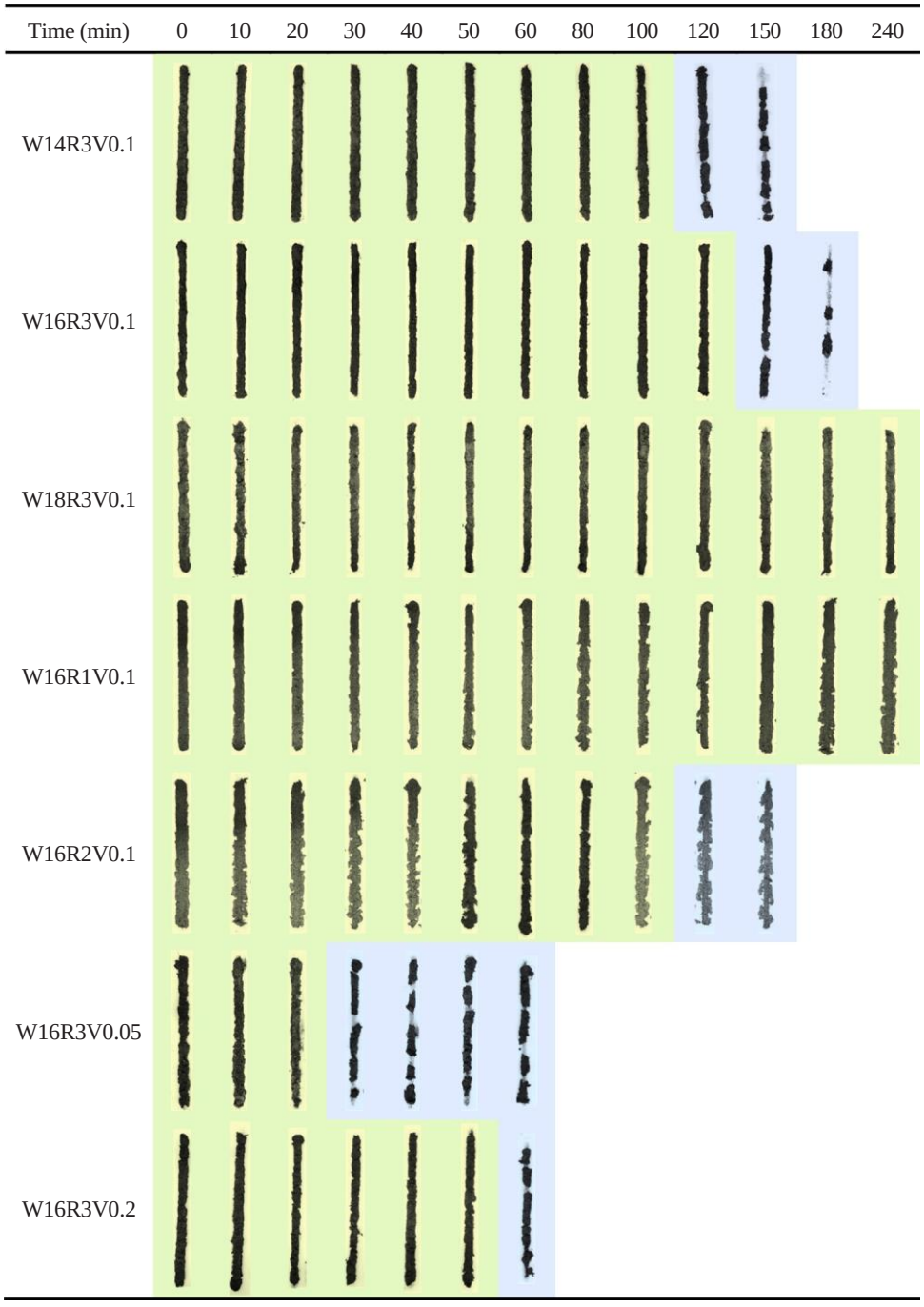

increases with higher w/b ratios. As the w/b ratio increases from 0.14 to 0.18, the printable time increases from 100 to 240 min. As the RSF content increases, the printable time of the mixture decreases, with a mixture with an RSF volume fraction of 3 % having half the printable time of a mixture with an RSF volume fraction of 1 %. However, unlike the effects of w/b ratio and RSF content on the printable time of the mixture, the printable time of the mixture shows an increasing and then decreasing trend as the VMA content increases. The printable time of the mixture with a VMA content of 0.2 % is 50 min, the printable time of the mixture with a VMA content of 0.1 % is 120 min, and the printable time of the mixture with a VMA content of 0.05 % is only 20 min. This is mainly because the lower amount of VMA results in poor bonding of the mixture and fractures within 30 min. In summary, except for mixtures of W16R3V0.05 and W16R3V0.2, all the mixtures can be printed for more than 60 min. Combining the results of the slump test and the printable time test, 20 min can be used as the opening time for extrudability and buildability testing of 3D printing RSF-reinforced UHPC.

3.3.2. Printable filament conformability

The key to ensuring a smooth and continuous 3D concrete printing process is that the concrete material needs to have excellent extrudability. The superior extruded printing filament should be characterized

by a continuous and uniform line with a width that is nearly or slightly larger than the diameter of the printhead [47]. Fig. 9 shows the test results of extruded filament conformability of 3D printing RSF-reinforced UHPC with different influencing factors. The influence of w/b ratio on extruded filament conformability is shown in Fig. 9(a). The results are analogous to the results of the slump and printable time tests in the previous section, the difference in extruded filament conformability between the mixtures having a w/b ratio of 0.14 and 0.16 is not significant, and the extrudate width of filaments is essentially the same as that of the design width. However, the width of the extruded filaments of the mixture with a w/b ratio of 0.18 is different from the design width.

Fig. 9(b) shows the influence of RSF volume fraction on the extruded filament conformability for 3D printing RSF-reinforced UHPC. The results show that the RSF content has little effect on the extruded filament conformability, and the results of the extruded width of each group of extruded filaments are almost the same, and the extruded width of the 3-filament group is wider than that of the design width by 6.01 %-8.83 % relative to the design width. Fig. 9(c) shows the influence of VMA content on the extruded filament conformability. The extruded width of the 0.1 % and 0.2 % VMA mixtures do not differ much from the design width, and the extruded width of the 3-filament group is 6.00 % and 6.66 % wider than the design width, respectively. The extruded width of the 0.05 % VMA mixtures differs considerably from the design width, with the 3-filament group having an extruded width 22.5 % wider than the design width.

3.4. Buildability

3.4.1. Buildable layers

Fig. 10 shows the comparative results for buildable layers and height of 3D printing RSF-reinforced UHPC. The results show that the mixture having a w/b ratio of 0.16 has a higher number of buildable layers and height, which can be vertically stacked up to 29 layers with a buildable height of 285 mm, whereas the mixtures having w/b ratios of 0.14 and 0.18 can be vertically stacked up to a height of no more than 145 mm. The major factor is that the mixture has higher dynamic yield strength when the w/b ratio is 0.14, increasing the dynamic yield stress directly leads to the weakening of the slurry flow, which is more difficult to flow because of the higher dynamic yield stress [61], and thus clogging occurs when it is printed to the 15th layer. However, the static yield stress of the mixture is lower in the case of a w/b ratio of 0.18, so only 15 layers can be stacked in the vertical direction.

Unlike the impact of the w/b ratio, the mixture has better buildability as RSF content is increased. As the volume fraction of RSF is increased from 1 % to 3 %, the number of vertically stackable layers of the mixture increases by 81.25 %. VMA content has a similar effect on the 3D printing RSF-reinforced UHPC buildability as RSF. When the VMA content is increased from 0.05 % to 0.2 %, the stackable height of the mixture increases by 57.56 %. These observations are consistent

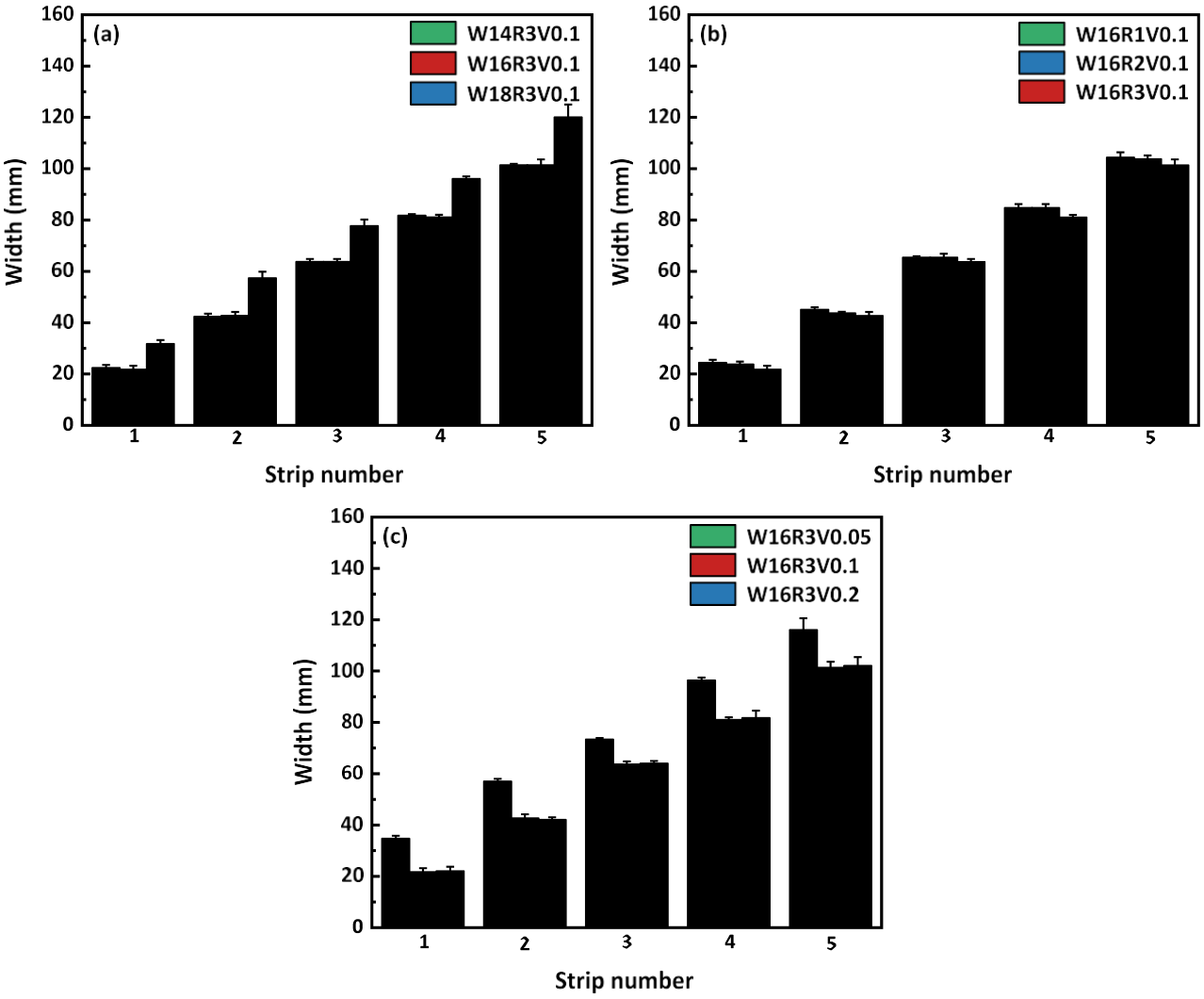

Fig. 9. Width of extruded filament for different groups of 3D printing mixture.

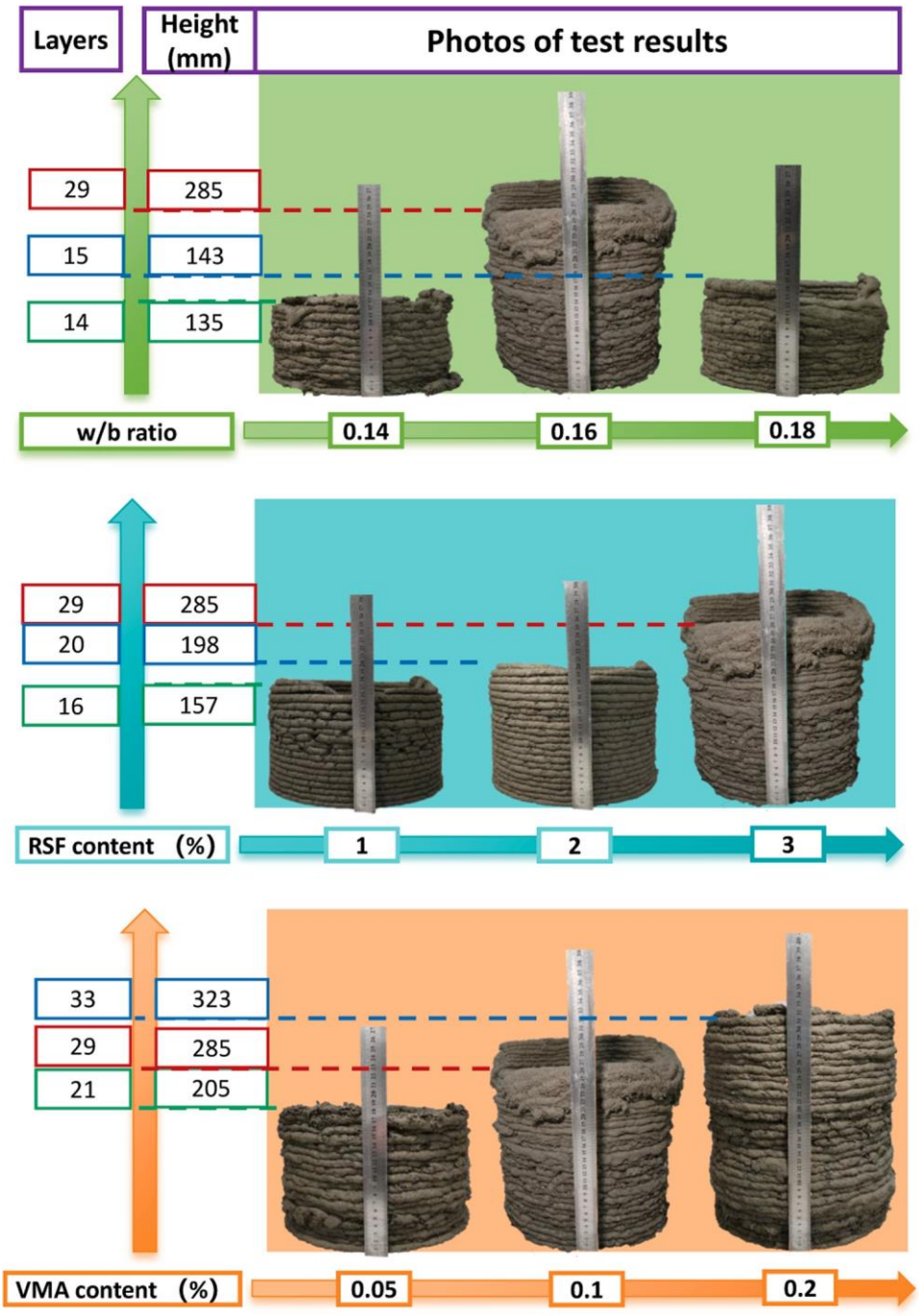

Fig. 10. Results of buildable layers and height tests of 3D printing mixture.

with the previous measurements of the rheological behaviour of 3D printing RSF-reinforced UHPC.

3.4.2. The layer settlement performance

When the print samples are stacked at a height comparable to or slightly below the model height, good buildability is ensured [47,62]. From Fig. 11, it is evident that the stability of the mixture during the building process is reduced by increasing the w/b ratio from 0.14 to 0.18. The mixture stability for the w/b ratios of 0.14 and 0.16 is nearly the same, with the shape stability ratios of 0.961 and 0.951, respectively. Increasing RSF and VMA content improves the stability of the mixture. To be more specific, the shape stability ratio of the mixture increases by 2.49 % when the RSF volume fraction is increased from 1 % to 3 %, and the shape stability ratio of the mixture increases by 6.30 % when the VMA content is increased from 0.05 % to 0.2 %.

3.5. Shape retention ability

Fig. 12 shows the SRA test photos of 3D printing RSF-reinforced UHPC specimens under vertical loading. When the VMA content increases from 0.05 % to 0.1 %, the load that the mixture can withstand increases by 147.82 %. In addition, the mixtures with 0.1 % and 0.2 % VMA can withstand the maximum loads in the test. Fig. 13 plots the variation curves of SRA indices (SRA_d and SRA_h) of 3D printing RSF-reinforced UHPC under vertical loading. With increasing vertical loading, the vertical and horizontal deformations (SRA_d and SRA_h) of

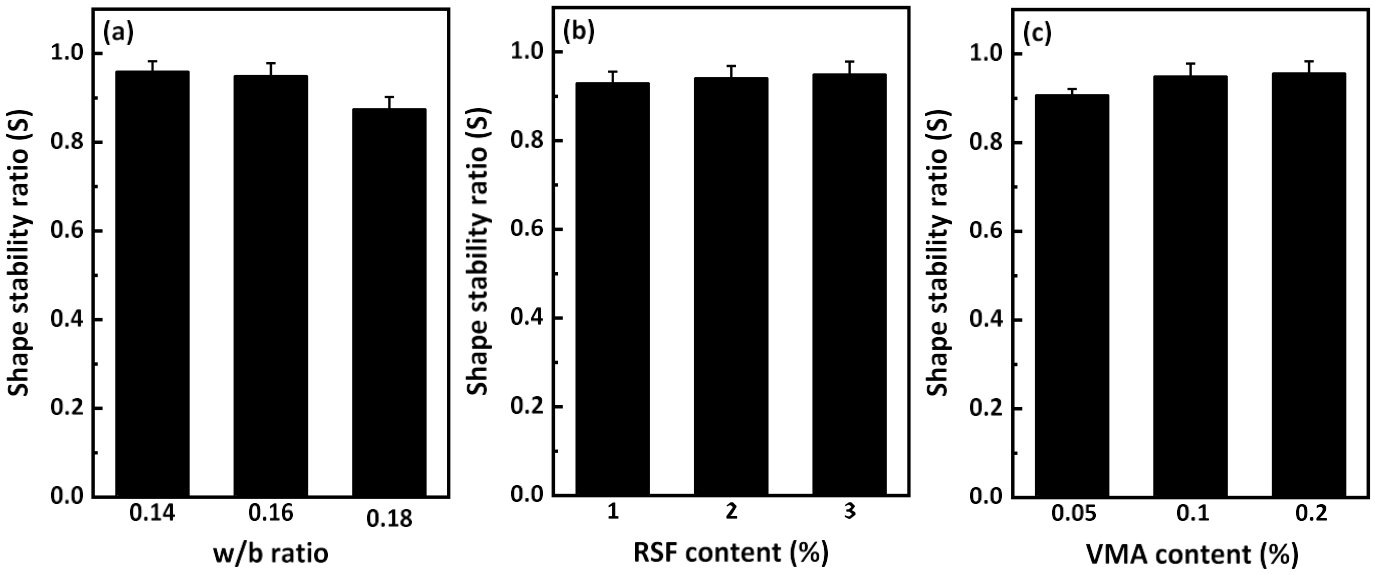

Fig. 11. Test results of 3D printing mixture printing five-layer objects.

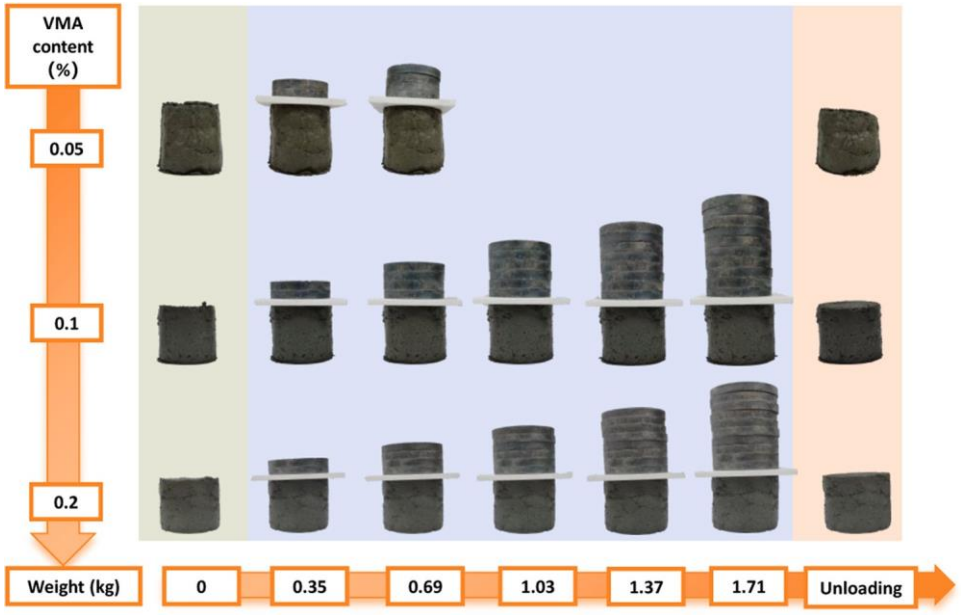

Fig. 12. Shape-retention-ability test results of 3D printing RSF-reinforced UHPC.

different influencing factor mixtures show different trends. Fig. 13(a) shows the influence of the w/b ratio on the SRA of 3D printing mixture under vertical loading, and it can be observed that the mixture specimens having w/b ratios 0.14 and 0.16 are damaged by vertical loads greater than about 1.71 kg, which is higher than the 1.03 kg load on the mixture specimen with w/b ratio 0.18. The influence of RSF content and VMA content on the SRA of the mixture are shown in Fig. 13(b) and Fig. 13(c). The results show that the influence of fibre content and VMA content on the SRA of the 3D printing mixture under vertical loading is similar, and the SRA of the mixture gradually increases with the gradual increase of the content, and the mixture has a higher vertical loading capacity. The mixtures W16R1V0.1 and W16R3V0.05 have similar load-carrying capacities, both breaking under a vertically applied load of around 0.69 kg, which is below the loading that specimens of the mixtures with the other contents can withstand (i.e., 1.71 kg). Thus, lower water binder ratios, usage of steel fibre and VMA can increase SRA and improve the ability of 3D printing mixture to withstand vertical loads.

3.6. 3D printability evaluation and mechanism evolution

3.6.1. 3D printability evaluation

The quantitative evaluation of flowability, extrudability, buildability and shape retention ability of 3D printing RSF-reinforced UHPC is shown in Fig. 14. Among them, flowability is evaluated through spread diameter, extrudability is evaluated by taking the results of printable time test and printable filament shape retention test, buildability is evaluated by test results of buildable time (slump test) and buildable layers test, and shape retention ability is evaluated by sustaining vertical loads. There are no uniform standards for the printability evaluation of 3D printing RSF-reinforced UHPC, and here we evaluate the printability of 3D printing RSF-reinforced UHPC using the relevant test results of W16R3V0.1 mixture as a benchmark.

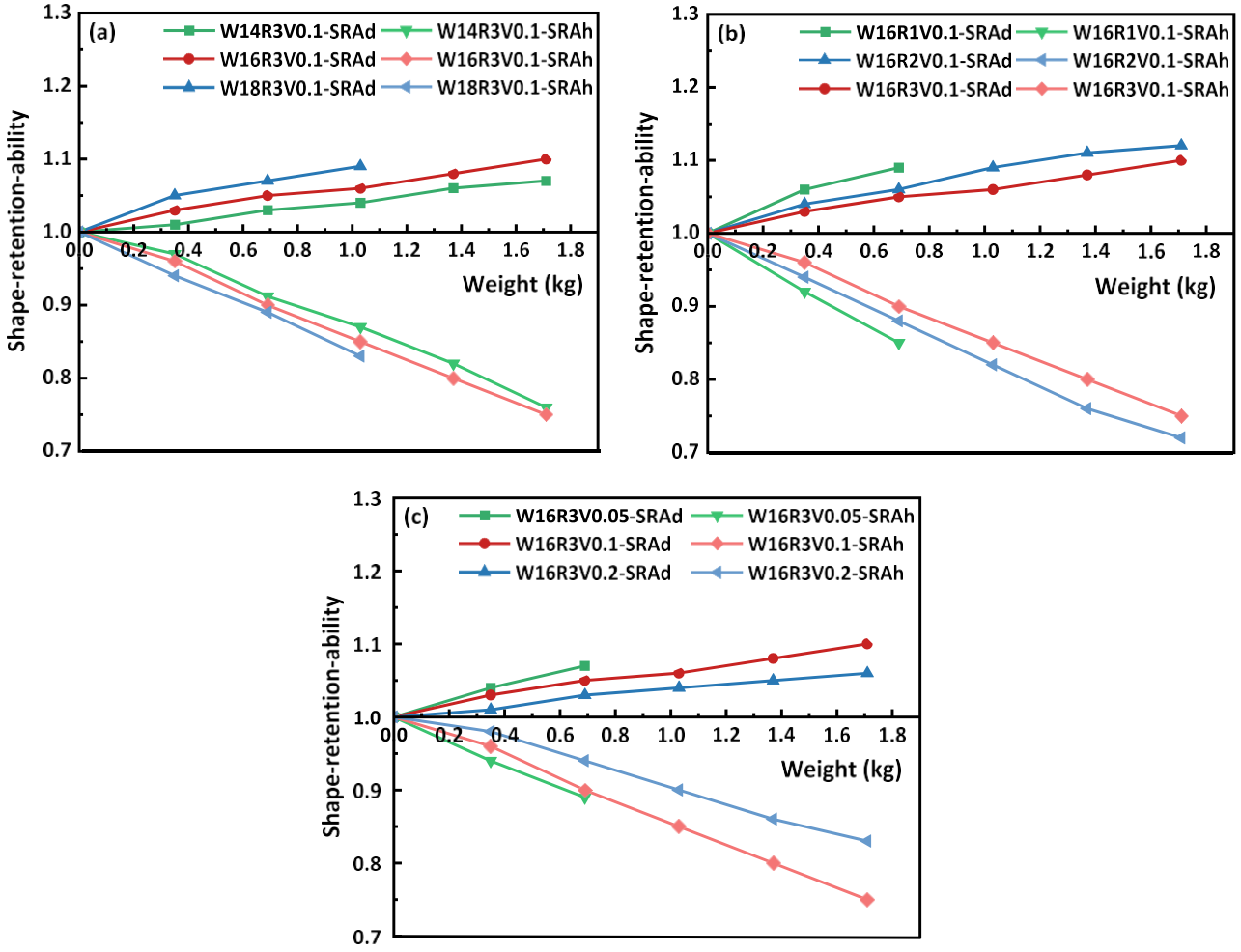

Fig. 13. Shape-retention-ability indices of 3D printing RSF-reinforced UHPC.

The 3D printing environment places stringent requirements on the printability of 3D concrete printing. The main reasons for this are as follows: (i) 3D concrete printing needs to have sufficient printable time to ensure that the material has enough time for initial curing after extrusion to form a stable interlayer bond, preventing interruption of printing and structural collapse [44]. At the same time, this also provides the operator with a window of time to adjust the printing parameters and respond to unexpected conditions, ensuring printing process continuity and printing quality stability. In addition, the sufficient printable time also adapts to the curing characteristics of concrete under different environmental conditions, enhancing the reliability and application range of 3D concrete printing technology. (ii) There is no formwork in the process of 3D printing, the printing material needs to bear its gravity alone and the vertical load of the subsequent printing material during the printing process. During the layer-by-layer stacking printing process, each layer of concrete must be accurately moulded and maintain its design shape to ensure that the overall structure is consistent with the design intent, thus requiring good shape retention. In summary, 3D printing RSF-reinforced UHPC having a w/b ratio of 0.16, RSF volume fraction of 3 % and VMA content of 0.1 % has good printability.

3.6.2. Evolutionary mechanisms of fresh mixture

Fig. 15 divides the mechanistic evolution of 3D printing RSF-reinforced UHPC fresh properties into three stages. Stage I (see Fig. 15b): 3D printing RSF-reinforced UHPC matrix particles are dispersed at the end of the mixing phase (Fig. 15a), and over time, small particles are aggregated into larger clusters by flocculation to form a colloidal interaction permeation network, during which VMA dissolves and hydration products nucleate [56]. This process occurs mainly within 30 min after hydration [63] and corresponds to the rapid linear growth of static yield stress in Fig. 5. Stage II (see Fig. 15c): VMA adsorption to particle surfaces, growth of hydration products, C-S-H nucleation at the pseudo-contacts of the particles, formation of bigger clusters by connecting the particles, as well as a shift from localized colloidal interactions to more stringent interactions [64]. Specifically, in the slump test, the slump values of the mixture after 30 min are all below 8 mm, and all of them have good conformability. At the same time, the mixture has a good ability to extrude filaments and withstand vertical loads. Stage III (see Fig. 15d): With time, the VMA stretches and bridges, the hydration products continue to grow, the size and the number of C-S-H bridges increase, and the system grows in size. This phase can be considered as a hardening phase [65], which occurs after 60 min and corresponds to the fact that the vast majority of mixtures do not fracture until after 60 min.

4. Conclusions

In this study, the rheological behaviour, flowability, extrudability, buildability and shape retention ability of 3D printing RSF-reinforced UHPC is investigated by varying the w/b ratios, RSF content and VMA content. The main conclusions are drawn as follows:

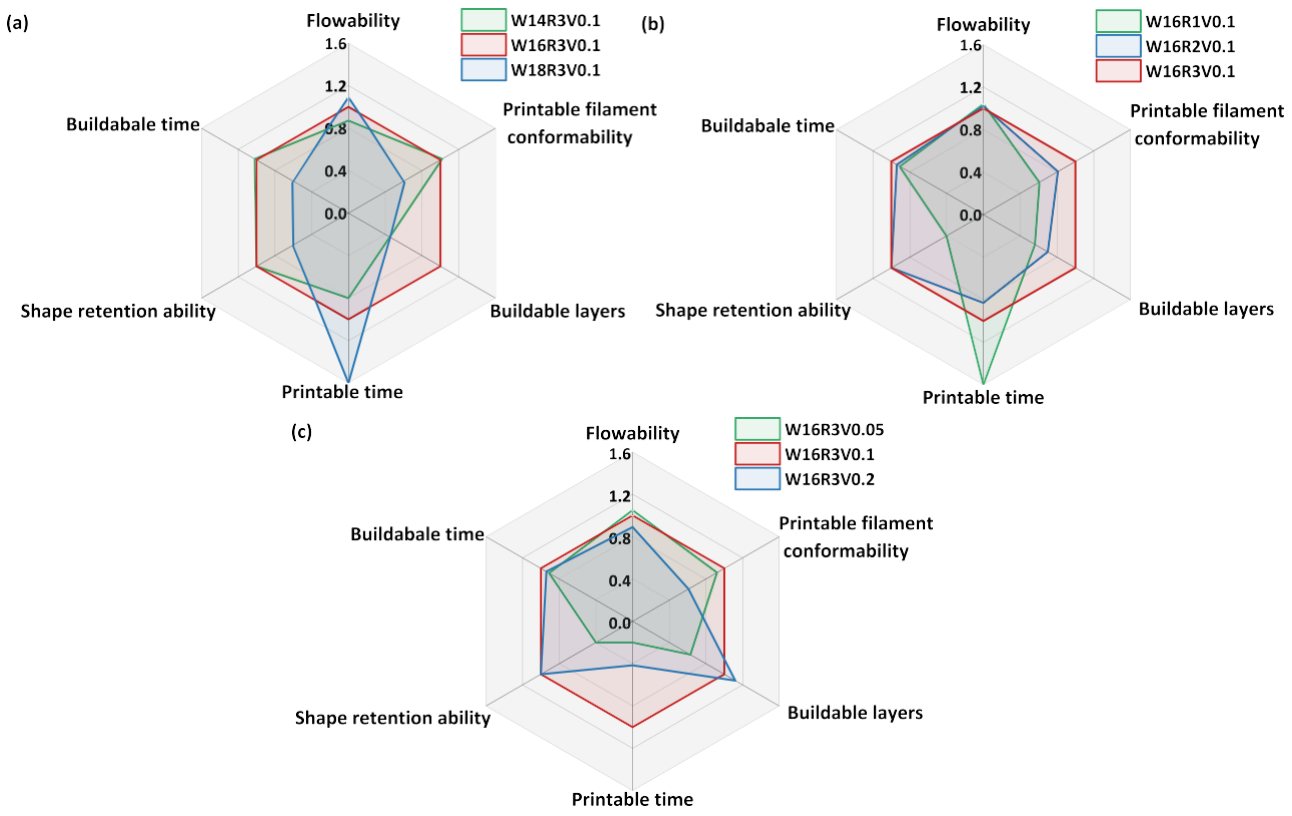

Fig. 14. 3D printability evaluation of RSF-reinforced UHPC.

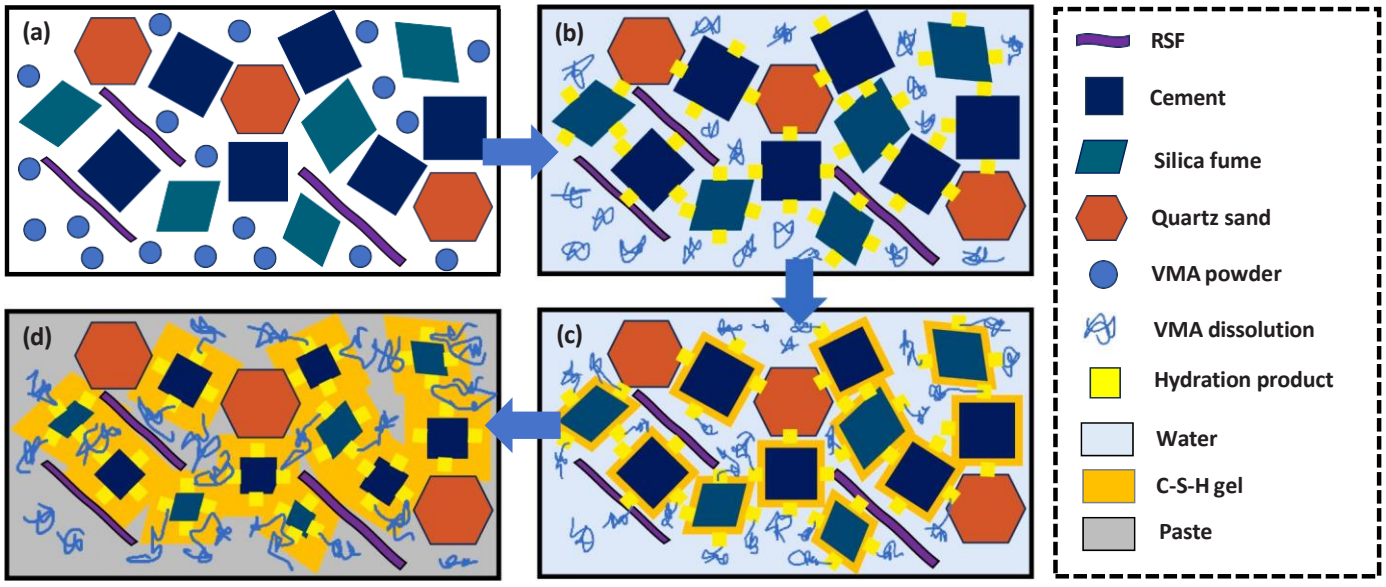

Fig. 15. Schematic illustration of the evolution of interaction of fresh 3D printing RSF-reinforced UHPC matrix: (a) Initial state, (b) Stage I, (c) Stage II and (d) Stage III.

- The reduction of the w/b ratio and the increase of the RSF or VMA content increase the static and dynamic yield stresses and the plastic viscosity of the mixture, while also reducing the slump and flowability of the mixture. The dynamic yield stress of the mixture increases by 27.37 % when the volume fraction of RSF is increased from 1 % to 3 % at the same w/b ratio and VMA content. This is mainly because the friction between RSF and the interaction of RSF with solid material reduces the packing density of the UHPC matrix.
- The printable time of the mixture can be extended both by decreasing the w/b ratio and by increasing the RSF volume fraction. However, as the VMA content increases, the printable time of the mixture tends to increase and then decrease. This is related to the poor bonding of the mixture due to the lower VMA contents. The difference in extruded filament conformability between mixtures with w/b ratios of 0.14 and 0.16 is not significant, whereas the extruded filament

width of mixtures with a w/b ratio of 0.18 differs considerably from the design width.

- The increasing content of RSF and VMA improves the buildability and shape retention ability of the mixture. As the volume fraction of RSF is increased from 1 % to 3 %, the number of vertically stackable layers of the mixture increases by 81.25 % and the S-value of the mixture increases by 2.49 %. These observations are consistent with the previously discussed measurements of the rheological behaviour of 3D printing RSF-reinforced UHPC.
- The mechanistic evolution of fresh properties of 3D printing RSF-reinforced UHPC goes through particle dispersion, colloidal agglomerate formation, and hydration product growth, which involves VMA dissolution and adsorption, as well as C-S-H formation and extension. Finally, the printability of the mixture is evaluated by a combination of extrudability, buildability and shape retention ability. The results show that the 3D printing RSF-reinforced UHPC with a w/b ratio of 0.16, 3 % volume fraction of RSF and 0.1 % VMA content has excellent printability.

The results of this study demonstrate the feasibility of 3D printing RSF-reinforced UHPC, and further research will be conducted to investigate the effect of the length distribution of RSF on the printability, as well as compare the effect of RSF and commercially available fibre on the printability of UHPC mixtures.

CRediT authorship contribution statement

Meng Chen: Writing – original draft, Methodology, Funding acquisition, Conceptualization. **Jiahui Li:** Writing – original draft, Validation, Investigation, Data curation. **Tong Zhang:** Writing – original draft, Visualization, Validation, Formal analysis. **Mingzhong Zhang:** Writing – review & editing, Formal analysis.

Declaration of Competing Interest

The authors declare that they have no known competing financial interests or personal relationships that could have appeared to influence the work reported in this paper.

Acknowledgements

The authors gratefully acknowledge the financial support from the Liaoning Provincial Natural Science Foundation (2024-MSBA-28), and the Fundamental Research Funds for the Central Universities (N2401001).

Data availability

Data will be made available on request.

References

[1] R.A. Buswell, W.R. Leal de Silva, S.Z. Jones, J. Dirrenberger, 3D printing using concrete extrusion: a roadmap for research, Cem. Concr. Res. 112 (2018) 37–49, https://doi.org/10.1016/j.cemconres.2018.05.006.

[2] T. Wangler, N. Roussel, F.P. Bos, T.A.M. Salet, R.J. Flatt, Digital concrete: a review, Cem. Concr. Res. 123 (2019), https://doi.org/10.1016/j.cemconres.2019.105780.

[3] Y. Chen, C. Romero Rodriguez, Z. Li, B. Chen, O. Çopurog˘lu, E. Schlangen, Effect of different grade levels of calcined clays on fresh and hardened properties of ternary-blended cementitious materials for 3D printing, Cem. Concr. Compos. 114 (2020), https://doi.org/10.1016/j.cemconcomp.2020.103708.

[4] M. Bi, P. Tran, L. Xia, G. Ma, Y.M. Xie, Topology optimization for 3D concrete printing with various manufacturing constraints, Addit. Manuf. 57 (2022) 102982, https://doi.org/10.1016/j.addma.2022.102982.

[5] C. Borg Costanzi, Z.Y. Ahmed, H.R. Schipper, F.P. Bos, U. Knaack, R.J.M. Wolfs, 3D Printing Concrete on temporary surfaces: the design and fabrication of a concrete shell structure, Autom. Constr. 94 (2018) 395–404, https://doi.org/10.1016/j.autcon.2018.06.013.

[6] M. Batikha, R. Jotangia, M.Y. Baaj, I. Mousleh, 3D concrete printing for sustainable and economical construction: a comparative study, Autom. Constr. 134 (2022) 104087, https://doi.org/10.1016/j.autcon.2021.104087.

[7] Y. He, Y. Zhang, C. Zhang, H. Zhou, Energy-saving potential of 3D printed concrete building with integrated living wall, Energy Build. 222 (2020) 110110, https://doi.org/10.1016/j.enbuild.2020.110110.

[8] G. De Schutter, K. Lesage, V. Mechtcherine, V.N. Nerella, G. Habert, I. Agusti-Juan, Vision of 3D printing with concrete — technical, economic and environmental potentials, Cem. Concr. Res. 112 (2018) 25–36, https://doi.org/10.1016/j.cemconres.2018.06.001.

[9] M.A. Hossain, A. Zhumabekova, S.C. Paul, J.R. Kim, A review of 3D printing in construction and its impact on the labor market, Sustain 12 (2020) 1–21, https://doi.org/10.3390/su12208492.

[10] V. Mechtcherine, J. Grafe, V.N. Nerella, E. Spaniol, M. Hertel, U. Füssel, 3D-printed steel reinforcement for digital concrete construction – manufacture, mechanical properties and bond behaviour, Constr. Build. Mater. 179 (2018) 125–137, https://doi.org/10.1016/j.conbuildmat.2018.05.202.

[11] E.L. Kreiger, M.A. Kreiger, M.P. Case, Development of the construction processes for reinforced additively constructed concrete, Addit. Manuf. 28 (2019) 39–49, https://doi.org/10.1016/j.addma.2019.02.015.

[12] J. Xiao, G. Ji, Y. Zhang, G. Ma, V. Mechtcherine, J. Pan, L. Wang, T. Ding, Z. Duan, S. Du, Large-scale 3D printing concrete technology: current status and future opportunities, Cem. Concr. Compos. 122 (2021) 104115, https://doi.org/10.1016/j.cemconcomp.2021.104115.

[13] C.-C. Hung, S. El-Tawil, S.-H. Chao, A review of developments and challenges for UHPC in structural engineering: behavior, analysis, and design, J. Struct. Eng. 147 (2021) 1–19, https://doi.org/10.1061/(asce)st.1943-541x.0003073.

[14] T. Zhang, J. Cui, M. Chen, J. Yang, Z. Yan, M. Zhang, Durability of concrete containing carbonated recycled aggregates: a comprehensive review, Cem. Concr. Compos. 156 (2025) 105865, https://doi.org/10.1016/J.CEMCONCOMP.2024.105865.

[15] C. Shi, Z. Wu, J. Xiao, D. Wang, Z. Huang, Z. Fang, A review on ultra high performance concrete: part I. Raw materials and mixture design, Constr. Build. Mater. 101 (2015) 741–751, https://doi.org/10.1016/j.conbuildmat.2015.10.088.

[16] T. Zhang, M. Zhang, Y. Shen, H. Zhu, Z. Yan, Mitigating the damage of ultra-high performance concrete at elevated temperatures using synergistic flame-retardant polymer fibres, Cem. Concr. Res. 158 (2022) 106835, https://doi.org/10.1016/j.cemconres.2022.106835.

[17] T. Zhang, H. Wang, M. Chen, L. Niu, W. Zhu, Effect of interfacial characteristics on dynamic splitting behavior of quasi rock-concrete composite layer: towards resilient tunnel support against rock burst, Tunn. Undergr. Sp. Technol. Inc. Trench Technol. Res. 155 (2024) 106134, https://doi.org/10.1016/j.tust.2024.106134.

[18] W. Yu, C. Xie, L. Jin, X. Du, Effects of fiber characteristics and specimen sizes on static and dynamic split-tensile failures of BFLAC: 3D mesoscopic simulations, Eng. Fract. Mech. 295 (2024) 109759, https://doi.org/10.1016/J.ENGFRACMECH.2023.109759.

[19] Y. Yang, C. Wu, Z. Liu, H. Zhang, 3D-printing ultra-high performance fiber-reinforced concrete under triaxial confining loads, Addit. Manuf. 50 (2022) 102568, https://doi.org/10.1016/j.addma.2021.102568.

[20] Y. Yang, C. Wu, Z. Liu, Rate dependent behaviour of 3D printed ultra-high performance fibre-reinforced concrete under dynamic splitting tensile, Compos. Struct. 309 (2023) 116727, https://doi.org/10.1016/j.compstruct.2023.116727.

[21] A.R. Arunothayan, B. Nematollahi, R. Ranade, S.H. Bong, J. Sanjayan, Development of 3D-printable ultra-high performance fiber-reinforced concrete for digital construction, Constr. Build. Mater. 257 (2020) 119546, https://doi.org/10.1016/j.conbuildmat.2020.119546.

[22] Y. Yang, C. Wu, Z. Liu, J. Li, T. Yang, X. Jiang, Characteristics of 3D-printing ultra-high performance fibre-reinforced concrete under impact loading, Int. J. Impact Eng. 164 (2022) 104205, https://doi.org/10.1016/j.ijimpeng.2022.104205.

[23] G. Bai, L. Wang, F. Wang, G. Ma, In-process reinforcing method: dual 3D printing procedure for ultra-high performance concrete reinforced cementitious composites, Mater. Lett. 304 (2021) 130594, https://doi.org/10.1016/j.matlet.2021.130594.

[24] L. Dong, Y. Yang, Z. Liu, Q. Ren, J. Li, Y. Zhang, C. Wu, Microstructure and mechanical behaviour of 3D printed ultra-high performance concrete after elevated temperatures, Addit. Manuf. 58 (2022) 103032, https://doi.org/10.1016/j.addma.2022.103032.

[25] M.N. Isa, K. Pilakoutas, M. Guadagnini, H. Angelakopoulos, Mechanical performance of affordable and eco-efficient ultra-high performance concrete (UHPC) containing recycled tyre steel fibres, Constr. Build. Mater. 255 (2020) 119272, https://doi.org/10.1016/J.CONBUILDMAT.2020.119272.

[26] A. Simalti, A.P. Singh, Comparative study on performance of manufactured steel fiber and shredded tire recycled steel fiber reinforced self-consolidating concrete, Constr. Build. Mater. 266 (2021) 121102, https://doi.org/10.1016/j.conbuildmat.2020.121102.

[27] M. Chen, J. Sun, T. Zhang, Y. Shen, M. Zhang, Enhancing the dynamic splitting tensile performance of ultra-high performance concrete using waste tyre steel fibres, J. Build. Eng. 80 (2023) 108102, https://doi.org/10.1016/j.jobe.2023.108102.

[28] M.R. Khosravani, Inverse characterization of UHPC material based on Hopkinson bar test, Appl. Eng. Sci. 6 (2021) 100043, https://doi.org/10.1016/j.apples.2021.100043.

[29] T. Zhang, J. Yang, M. Chen, P. Gao, M. Zhang, Effect of iron tailing fines on dynamic properties and microstructure of recycled steel fibre reinforced ultra-high performance concrete Data from China Mineral, Constr. Build. Mater. 460 (2025) 139679, https://doi.org/10.1016/j.conbuildmat.2024.139679.

[30] A. Sofi, Effect of waste tyre rubber on mechanical and durability properties of concrete – a review, Ain Shams Eng. J. 9 (2018) 2691–2700, https://doi.org/10.1016/j.asej.2017.08.007.
[31] F.A.Ismail Fauzan, R. Sandi, N. Syah, A.P. Melinda, The effects of steel fibers extracted from waste tyre on concrete containing palm oil fuel ash, Int. J. Geomate. 14 (2018) 142–148, https://doi.org/10.21660/2018.44.3563.
[32] M.A. Aiello, F. Leuzzi, G. Centonze, A. Maffezzoli, Use of steel fibres recovered from waste tyres as reinforcement in concrete: pull-out behaviour, compressive and flexural strength, Waste Manag 29 (2009) 1960–1970, https://doi.org/10.1016/j.wasman.2008.12.002.
[33] M. Leone, G. Centonze, D. Colonna, F. Micelli, M.A. Aiello, Fiber-reinforced concrete with low content of recycled steel fiber: shear behaviour, Constr. Build. Mater. 161 (2018) 141–155, https://doi.org/10.1016/j.conbuildmat.2017.11.101.
[34] G. Centonze, M. Leone, M.A. Aiello, Steel fibers from waste tires as reinforcement in concrete: a mechanical characterization, Constr. Build. Mater. 36 (2012) 46–57, https://doi.org/10.1016/j.conbuildmat.2012.04.088.
[35] H. Zhong, M. Chen, M. Zhang, Effect of hybrid industrial and recycled steel fibres on static and dynamic mechanical properties of ultra-high performance concrete, Constr. Build. Mater. 370 (2023) 130691, https://doi.org/10.1016/j.conbuildmat.2023.130691.
[36] P. Richard, M. Cheyrezy, Composition of reactive powder concretes, Cem. Concr. Res. 25 (1995) 1501–1511, https://doi.org/10.1016/0008-8846(95)00144-2.
[37] G. Bai, L. Wang, F. Wang, G. Ma, Assessing printing synergism in a dual 3D printing system for ultra-high performance concrete in-process reinforced cementitious composite, Addit. Manuf. 61 (2023) 103338, https://doi.org/10.1016/j.addma.2022.103338.
[38] D. Feys, J.E. Wallevik, A. Yahia, K.H. Khayat, O.H. Wallevik, Extension of the Reiner-Riwlin equation to determine modified Bingham parameters measured in coaxial cylinders rheometers, Mater. Struct. Constr. 46 (2013) 289–311, https://doi.org/10.1617/s11527-012-9902-6.
[39] U. Boddepalli, I.S.R. Gandhi, B. Panda, Synergistic effect of fly ash and polyvinyl alcohol fibers in improving stability, rheology, and mechanical properties of 3D printable foam concrete, Constr. Build. Mater. 429 (2024) 136464, https://doi.org/10.1016/j.conbuildmat.2024.136464.
[40] E.C. Bingham, Fluidity and plasticity, McGraw-Hill, 1922 (pdf, (n.d.)).
[41] V.M.I. Ivanova, Evaluation of structural build-up rate of cementitious materials by means of constant shear rate test: parameter study, Rheol. Process. Constr. Mater. 23 (2019) 209–218, https://doi.org/10.1007/978-3-030-22566-7_62.
[42] K.H. Khayat, W. Meng, K. Vallurupalli, L. Teng, Rheological properties of ultra-high-performance concrete — An overview, Cem. Concr. Res. 124 (2019) 105828, https://doi.org/10.1016/j.cemconres.2019.105828.
[43] Test Method for Flowability of Cement Mortar, GB-T 2419-2005, Ministry of Housing and Urban-rural Development of the People's Republic of China, 2005., (n.d.).
[44] Y. Chen, K. Xia, Z. Jia, Y. Gao, Z. Zhang, Y. Zhang, Extending applicability of 3D-printable geopolymer to large-scale printing scenario via combination of sodium carbonate and nano-silica, Cem. Concr. Compos. 145 (2024) 105322, https://doi.org/10.1016/j.cemconcomp.2023.105322.
[45] T.T. Le, S.A. Austin, S. Lim, R.A. Buswell, A.G.F. Gibb, T. Thorpe, Mix design and fresh properties for high-performance printing concrete, Mater. Struct. Constr. 45 (2012) 1221–1232, https://doi.org/10.1617/s11527-012-9828-z.
[46] A.R. Arunothayan, B. Nematollahi, K.H. Khayat, A. Ramesh, J.G. Sanjayan, Rheological characterization of ultra-high performance concrete for 3D printing, Cem. Concr. Compos. 136 (2023) 104854, https://doi.org/10.1016/j.cemconcomp.2022.104854.
[47] Y. Chen, S. Chaves Figueiredo, Z. Li, Z. Chang, K. Jansen, O. Çopurog˘lu, E. Schlangen, Improving printability of limestone-calcined clay-based cementitious materials by using viscosity-modifying admixture, Cem. Concr. Res. 132 (2020), https://doi.org/10.1016/j.cemconres.2020.106040.
[48] Z. Liu, M. Li, Y. Weng, Y. Qian, T.N. Wong, M.J. Tan, Modelling and parameter optimization for filament deformation in 3D cementitious material printing using support vector machine, Compos. Part B Eng. 193 (2020) 108018, https://doi.org/10.1016/j.compositesb.2020.108018.
[49] I. Ivanova, V. Mechtcherine, Effects of volume fraction and surface area of aggregates on the static yield stress and structural build-up of fresh concrete, Mater. (Basel) 13 (2020), https://doi.org/10.3390/ma13071551.
[50] M. Zou, C. Liu, K. Zhang, W. Li, Q. Cao, L. Zhang, T. Gu, G. Zhang, L. Liu, Evaluation and control of printability and rheological properties of 3D-printed rubberized concrete, J. Build. Eng. 80 (2023) 107988, https://doi.org/10.1016/j.jobe.2023.107988.
[51] H. Gao, L. Jin, Y. Chen, Q. Chen, X. Liu, Q. Yu, Rheological behavior of 3D printed concrete: influential factors and printability prediction scheme, J. Build. Eng. 91 (2024) 109626, https://doi.org/10.1016/j.jobe.2024.109626.
[52] H. Bessaies-Bey, K.H. Khayat, M. Palacios, W. Schmidt, N. Roussel, Viscosity modifying agents: Key components of advanced cement-based materials with adapted rheology, Cem. Concr. Res. 152 (2022) 106646, https://doi.org/10.1016/j.cemconres.2021.106646.
[53] M. Rahman, S. Rawat, R. (Chunhui) Yang, A. Mahil, Y.X. Zhang, A comprehensive review on fresh and rheological properties of 3D printable cementitious composites, J. Build. Eng. 91 (2024) 109719, https://doi.org/10.1016/j.jobe.2024.109719.
[54] B. Zhou, Y. Uchida, Influence of flowability, casting time and formwork geometry on fiber orientation and mechanical properties of UHPFRC, Cem. Concr. Res. 95 (2017) 164–177, https://doi.org/10.1016/j.cemconres.2017.02.017.
[55] M. Sonebi, Rheological properties of grouts with viscosity modifying agents as diutan gum and welan gum incorporating pulverised fly ash, Cem. Concr. Res. 36 (2006) 1609–1618, https://doi.org/10.1016/j.cemconres.2006.05.016.
[56] N. Roussel, G. Ovarlez, S. Garrault, C. Brumaud, The origins of thixotropy of fresh cement pastes, Cem. Concr. Res. 42 (2012) 148–157, https://doi.org/10.1016/j.cemconres.2011.09.004.
[57] M. Chen, H. Si, X. Fan, Y. Xuan, M. Zhang, Dynamic compressive behaviour of recycled tyre steel fibre reinforced concrete, Constr. Build. Mater. 316 (2022) 125896, https://doi.org/10.1016/j.conbuildmat.2021.125896.
[58] C. Li, L. Miao, Q. You, S. Hu, H. Fang, Effects of viscosity modifying admixture (VMA) on workability and compressive strength of structural EPS concrete, Constr. Build. Mater. 175 (2018) 342–350, https://doi.org/10.1016/j.conbuildmat.2018.04.176.
[59] Y. Chen, S. He, Y. Zhang, Z. Wan, O. Çopurog˘lu, E. Schlangen, 3D printing of calcined clay-limestone-based cementitious materials, Cem. Concr. Res. 149 (2021), https://doi.org/10.1016/j.cemconres.2021.106553.
[60] Y.W.D. Tay, Y. Qian, M.J. Tan, Printability region for 3D concrete printing using slump and slump flow test, Compos. Part B Eng. 174 (2019) 106968, https://doi.org/10.1016/j.compositesb.2019.106968.
[61] Q. Yu, B. Zhu, X. Li, L. Meng, J. Cai, Y. Zhang, J. Pan, Investigation of the rheological and mechanical properties of 3D printed eco-friendly concrete with steel slag, J. Build. Eng. 72 (2023) 106621, https://doi.org/10.1016/j.jobe.2023.106621.
[62] C. Liu, X. Wang, Y. Chen, C. Zhang, L. Ma, Z. Deng, C. Chen, Y. Zhang, J. Pan, N. Banthia, Influence of hydroxypropyl methylcellulose and silica fume on stability, rheological properties, and printability of 3D printing foam concrete, Cem. Concr. Compos. 122 (2021) 104158, https://doi.org/10.1016/j.cemconcomp.2021.104158.
[63] Z. Zhang, Z. Jia, J. Shi, Y. Jiang, N. Banthia, Y. Zhang, Clarifying and quantifying the driving force for the evolution of static yield stress of cement pastes, Cem. Concr. Res. 167 (2023) 107129, https://doi.org/10.1016/j.cemconres.2023.107129.
[64] Y. Zhang, Q. Ren, X. Dai, Y. Tao, Y. Zhang, Z. Jiang, K. Van Tittelboom, G. De Schutter, A potential active rheology control approach for 3D printable cement-based materials: coupling of temperature and viscosity modifiers, Cem. Concr. Compos. 149 (2024) 105496, https://doi.org/10.1016/j.cemconcomp.2024.105496.
[65] Z. Guo, J. Qiu, L. Pel, Y. Zhao, Q. Zhu, J.W. Kwek, L. Zhang, H. Jiang, J. Yang, Z. Qu, A contribution to understanding the rheological measurement, yielding mechanism and structural evolution of fresh cemented paste backfill, Cem. Concr. Compos. 143 (2023) 105221, https://doi.org/10.1016/j.cemconcomp.2023.105221.